Hindawi
Shock and Vibration
Volume 2017, Article ID 8494657, 16 pages
https://doi.org/10.1155/2017/8494657

Research Article

Numerical Study on the In-Plane and Out-of-Plane Resistance of Brick Masonry Infill Panels in Steel Frames

Vahid Bahreini,[1] Tariq Mahdi,[2] and MohammadMahdi Najafizadeh[3]

[1]*Department of Civil Engineering, Arak Branch, Islamic Azad University, Arak, Iran*
[2]*Structural Engineering Department, BHRC, Tehran, Iran*
[3]*Department of Mechanical Engineering, Arak Branch, Islamic Azad University, Arak, Iran*

Correspondence should be addressed to Tariq Mahdi; mahdi@bhrc.ac.ir

Received 11 November 2016; Revised 13 April 2017; Accepted 7 May 2017; Published 28 May 2017

Academic Editor: Yuri S. Karinski

Masonry infill walls are one of the main forms of interior partitions and exterior walls in many parts of the world. Nevertheless, serious damage and loss of stability of many masonry infill walls had been reported during recent earthquakes. To improve their performance, the interaction between these infill walls and the bounding frames needs to be properly investigated. Such interaction can dramatically increase the stiffness of the frame in the in-plane direction. To avoid the negative aspects of inappropriate interactions between the frame and infill wall, some kind of isolation needs to be introduced. In this paper, three different configurations have been evaluated by using the general finite element software, ABAQUS. Nonlinear pushover and time history analyses have been conducted for each of the three configurations. Results showed that isolation of the infill from the frame has a significant effect on the in-plane response of infilled frames. Furthermore, adequate out-of-plane stability of the infill wall has been achieved. The results show that masonry infill walls that have full contact at the top of the wall but isolated from columns have shown acceptable performance.

1. Introduction

Brick masonry walls are subjected to both in-plane and out-of-plane loads during an earthquake excitation. Horizontal loading results in in-plane story shear forces, while the out-of-plane load is a result of either the out-of-plane inertial force caused by the considerable mass of the brick wall or the out-of-plane action of the flexible floor on the wall. Figure 1 shows the typical failure modes of masonry infill walls under in-plane loading, including the bed-joint sliding, diagonal tension failure, and corner compressive failure. In-plane response of the infill walls was extensively investigated in the literature in the past decades [1–4]. As for the out-of-plane failure of infill walls, a series of field observations from recent earthquakes such as the 1999 Kocaeli earthquake, Turkey, the 2009 L'Aquila earthquake, Italy, and the 2015 Gorkha earthquake, Nepal, has shown that this type of mechanism of masonry infills occurred quite often, indicating the need to introduce improved construction procedures [5–7].

Considerations should be taken into account in the new design guidelines with the focus on the out-of-plane performance of masonry infills in the design of infilled Reinforced Concrete (RC) structures subjected to earthquake loading [8]. Corresponding deficiencies need to be addressed in the earthquake design procedures for unreinforced masonry construction, where the out-of-plane response of walls is a key aspect of the seismic performance of the building [9].

Some design procedures still assume the collapse mechanism at the point of exceeding the wall's bending strength, while this typically occurs in bending at very small displacements. This was found by many researchers to be extremely conservative for seismic design of masonry infill walls [10, 11], which the collapse often corresponds to the bending displacements more than the thickness of the wall, typically about 100 mm for single leaf clay brick masonry [9].

Regarding the in-plane response of infill walls, current design guidelines have different provisions and recommendations for considering the probable effects of masonry infill

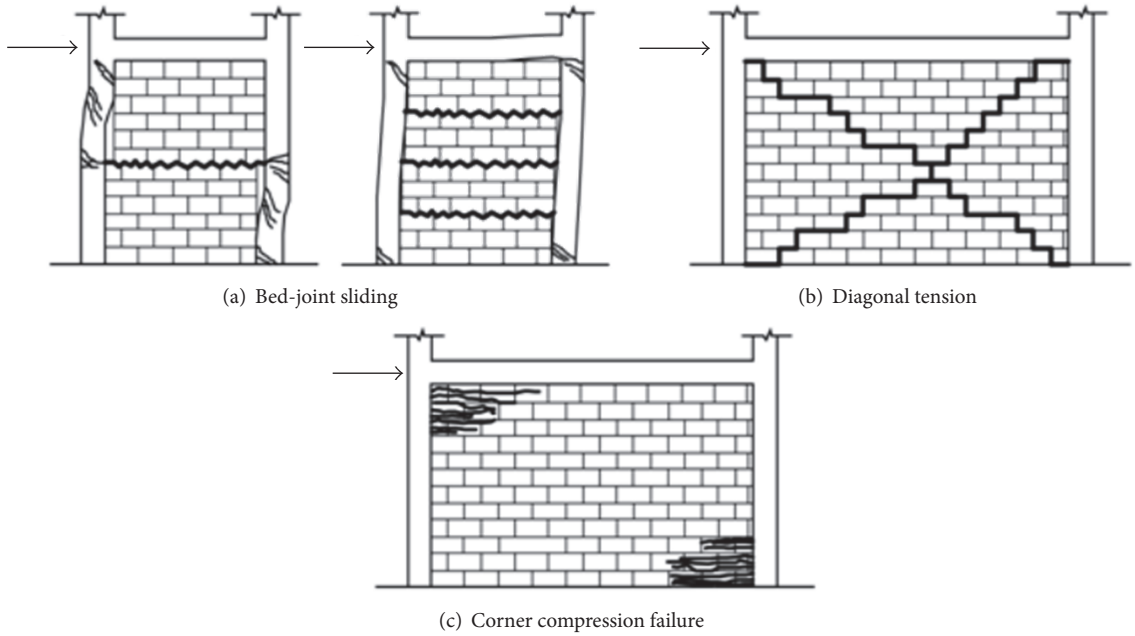

(a) Bed-joint sliding (b) Diagonal tension

(c) Corner compression failure

Figure 1: Typical failure modes of masonry infill walls under in-plane loading [15].

walls on the seismic performance of buildings. Some design codes ignore masonry infills and their contribution to the structure's strength and stiffness. Masonry walls confined with horizontal and vertical ties are able to mobilize a considerably higher stiffness as well as higher resistance to out-of-plane loads than the unconfined masonry walls. Confining effects can also affect the out-of-plane response of the infill wall and can lead to a considerable additional lateral capacity beyond first cracking due to arching of an infill wall confined within the frame [12]. This behavior was also confirmed by Flanagan and Bennett [13] and Asteris et al. [14].

In design of a structure according to the current design practices, distribution of forces and hence the demand in each structural component in seismic design of the building may notably vary from the design assumptions and code provisions. Recent studies have shown that infill walls can enhance the frame response even up to the expected story drift ratios presented by some design codes, for example, EuroCode 8 [18–20]. Specific provisions are specified in the current Chinese seismic design code (GB50011-2010) [21] to reduce the negative effect of the infill wall. Detailed modeling of infill wall in the analytical models, however, is not yet necessary according to these design codes. EuroCode 8 provisions include some fundamentals for spatial models for the analysis of the structure including infill walls in the case of severe irregularities in plan and in elevation. Regarding the frame-infill interactions, recommendations usually focus on the in-plane behavior of infilled frames only, and the out-of-plane behavior of infill walls has not received much attention.

In the current study, in-plane and out-of-plane responses of masonry infill walls were investigated through nonlinear finite element (FE) analyses using the general-purpose FE package, ABAQUS [22]. A parametric study was conducted to find the effective parameters on the in-plane and out-of-plane responses of isolated masonry infills in a typical steel frame and to find an efficient edge support configuration for the infill wall interface. Three frame-infill configurations were investigated, each with three different height-to-length ratios (H/L). Pushover analyses were conducted to evaluate the effects of infill configuration on the in-plane behavior of the frame. Moreover, the seismic out-of-plane response of the infill walls was investigated through time history analyses, using the Incremental Dynamic Analysis (IDA) method. Effects of different ground motion records, that is, the frequency content, were also studied.

2. Failure Modes of Masonry Infill Walls

2.1. Traditional Configuration. Frame structures with ordinary solid masonry infill walls were often found to have a poor deformation capacity during severe earthquakes. Investigation on the dynamic properties of infilled frames reveals that, compared to bare frames, these structural systems often experience higher levels of seismic force demands because of increasing the stiffness of the structure; however, presence of infill walls is effective in enhancing the lateral stiffness and strength of these structures which itself leads to lower experienced story drifts. Concentrated crack zone at the bottom of the wall causes the final brittle failure in the form of shear failure or crushing and consequently reduces the energy dissipation capacity of the structure.

Frames infilled with solid masonry bricks sometimes suffer from other potentially negative effects such as torsional effects and soft-story and weak-story mechanisms due the irregularities in plan and elevation, respectively. Moreover, stress concentration in the frame-infill wall interface is another issue that needs to be considered in design of infilled

frame structures [23]. The latter was found to be rarely investigated and addressed in the literature.

2.2. Isolated Configuration. Despite the reported experimental observations [1–4, 24–29] and the proposed analytical and numerical methods [30–38] in the past decades, a reliable consideration of the contribution of infill walls in seismic response of infilled frames is still difficult due to the structural uncertainties related to the sophisticated nature of masonry infill wall. Moreover, the variations in the interaction between the infill walls and the surrounding frame cannot be quantitatively described [29]. Since masonry infill walls are normally considered as nonstructural components, their effect is often ignored in design and evaluations. To overcome the mentioned disadvantages, separation of the infill wall from the surrounding frame was investigated and proposed by some researchers [39–43] and design codes [44, 45].

In the current study, three different configurations for the frame-infill interaction are considered to evaluate the effects of this interaction on the structural behavior of infilled steel frames with isolated infill walls, as follows:

(i) Infill wall isolated at the top and both sides, having three supporting points in the form of steel angles on both sides of each wall's edge (Case I).

(ii) Infill wall isolated at the top and both sides, having four supporting points on both sides of each wall's edge (Case II).

(iii) Infill wall isolated at the left and the right sides only, having four supporting points on both sides of each wall's edge (Case III).

All the three cases are analyzed with three different height-to-length ratios; $H/L = 1.0$, 0.75, and 0.6. A schematic layout of the three cases is presented in Figure 2.

3. Numerical Modeling

Details of the implemented FE model including the geometry of the models, the modeling approach, and the validation results are presented in this section. After the verification of the numerical model, this modeling approach was utilized to conduct the parametric study on the behavior of steel frames with solid masonry infill walls.

3.1. Models Geometrical Characteristics. The steel frame consists of IPB160 beams and columns with rigid connections and is connected to a stiff ground support. The height of the frame is kept constant as 3 m, and three different H/L ratios of 1.0, 0.75, and 0.6 are considered, resulting in span lengths of 3.0, 4.0, and 6.0 m, respectively. Infill walls consist of 200 × 200 × 100 mm bricks, and a 50 mm gap is considered on the infill wall edges to separate the infill from the moment frame. Steel angle supports ($L100 \times 10$) for each side of the infill wall are considered as a single piece with the length equal to 1000 mm (Case I) or in two pieces with the lengths of 500 mm (Cases II and III). Moreover, four shorter steel angles ($L = 300$ m) are used to support the corner regions of the wall for all the three configurations. Figure 3 shows a sample of the geometrical configuration of Case I in the current study.

3.2. Modeling Approach. The software package used for FE modeling in this study is the general-purpose nonlinear FE package ABAQUS, which offers comprehensive material constitutive laws and capable interaction features for simulation of masonry infill walls. Details of the geometry and element meshes, constitutive material models, and the numerical analyses are as follows.

3.2.1. Geometry and Mesh. Eight-node three-dimensional reduced integration elements with a Gaussian integration point in the element (C3D8R) are used for simulation of steel frame and solid bricks. Reduced integration elements need less computational time; however, in some cases, these elements are susceptible to hour glassing problem, which results in severe flexibility and no experienced strains at the integration points. The nonlinear solver in ABAQUS often prevents this situation by considering a small artificial stiffness [22]. Adjacent nodes in the steel parts in the model have been coupled using tie constraints to have perfect connections. As a result, no failure in the welds between the columns, beam, and angles is considered and these connections are assumed to behave ideally with no weakness.

The solid elements in the steel frame and angles had a dimension of approximately 200 mm. Compatible meshes are created for different parts of the model to have relatively ideal coupling in the tie constraints and also at the interface location of infill wall and the frame. Mesh sensitivity analyses are conducted to ensure the appropriateness of the selected mesh type and size. Figure 4 shows the employed mesh and the boundary conditions applied in the model for Case I. Similar mesh configurations are adopted for the other two cases.

3.2.2. Constitutive Material Models. There are a number of constitutive models available in the literature based on principles of elasticity, plasticity, and continuum damage mechanics. In the current study, Drucker-Prager model is used to define the mechanical properties of solid bricks in the model, based on the micro modeling technique proposed by Lourenco [30] and extended by Lourenço et al. [46]. However, the interactions between the bricks are modeled by interface behavior in the form of contact elements. The adopted strategy is shown in Figure 5(a).

The Drucker-Prager constitutive law for materials is capable of modeling frictional materials, which are typically granular-like soils and rocks and exhibit pressure-dependent yield as the material becomes stronger as the pressure increases. This material model is suitable for materials in which the compressive yield strength is greater than the tensile yield strength, such as those commonly found in composite materials, and allows the material to harden and soften [22]. Tables 1 and 2 show the mechanical properties of masonry bricks and shear interface parameters used in the parametric studies in the current work. These values are kept constant in the verification models, unless otherwise is specified. Compression hardening option is used for masonry bricks, starting from the yield stress equal to 3.12 MPa up to an ultimate stress of 5.2 MPa which correspond to the strain of 0.002.

Interactions between the masonry bricks are defined between the contact surfaces through adjusting the normal

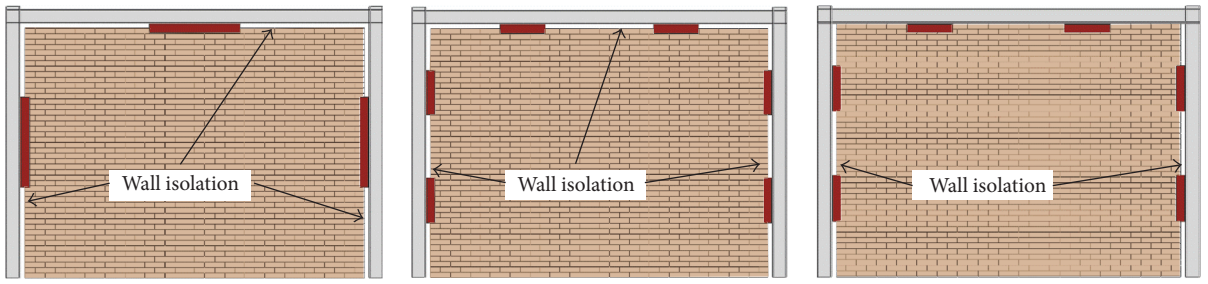

(a) Case I (b) Case II (c) Case III

Figure 2: Considered frame-infill configurations.

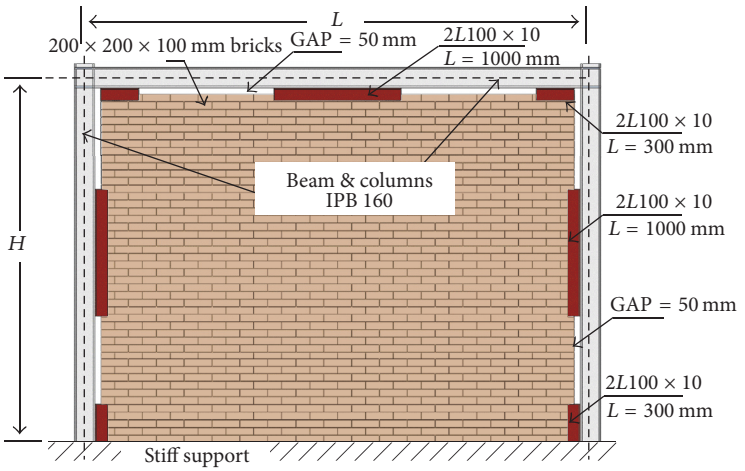

Figure 3: Sample geometrical configuration of Case I.

Table 1: Mechanical properties of masonry bricks.

Parameter	Value
Density, kg/m^3	1980
Modulus of elasticity, MPa	2550
Poisson's ratio	0.19
Friction angle (β), degrees	31.79
Dilation angle (ψ), degrees	2.86

and tangential behaviors. The latter supports a friction feature by which the transmission of the shear forces in the interface can be taken into account when two surfaces are in contact (Figure 5(b)). ABAQUS is able to account for the friction coefficient as a function of contact pressure. In this research, penalty formulation with a variable friction coefficient for masonry interaction peaking at 1.5 was defined based on the study by Bekloo [47]. As an example, friction coefficient between the masonry units was reported by Tasnimi and Mohebkhah [16] to be equal to 0.74 which is adopted in the verification of the mode under in-plane loading in Verification of the Numerical Model. This value is equal to the friction coefficient corresponding to the surface pressure of 1.61 MPa in the parametric study in this paper according to Bekloo [47].

Table 2 presents a summary of parameters used to define the tangential behavior of contact interfaces between the masonry units. The units are free to slide once the shear stress in the contact interface exceeded the maximum shear stress specified as mortar shear strength (Figure 5(b)). This method was previously proved to lead to reasonable results [47].

For the steel columns, beam, and angles, combined hardening plasticity is considered by providing the bilinear half cycle stress-strain data. The yield stress and the ultimate stress are considered as 240 MPa and 360 MPa, respectively.

3.2.3. Numerical Analysis. Two types of analysis are conducted in the study to evaluate the response of the infilled frames: quasi-static and dynamic time history analysis for in-plane and out-of-plane directions, respectively. Although the quasi-static situation could be simply provided by static analysis, nonlinear analyses in both cases are conducted using Explicit solver to reduce the convergence issues. In the in-plane direction, displacement controlled analysis is defined by applying a smooth stepping mode through the analysis in the way that properly provides a quasi-static situation. This method was also previously employed by other researchers [48, 49].

3.3. Verification of the Numerical Model. In this part, the in-plane and out-of-plane behavior of infilled frames are verified

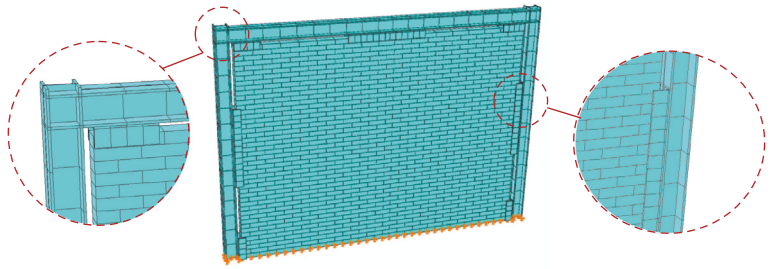

Figure 4: Finite element mesh and boundary conditions applied in the numerical model.

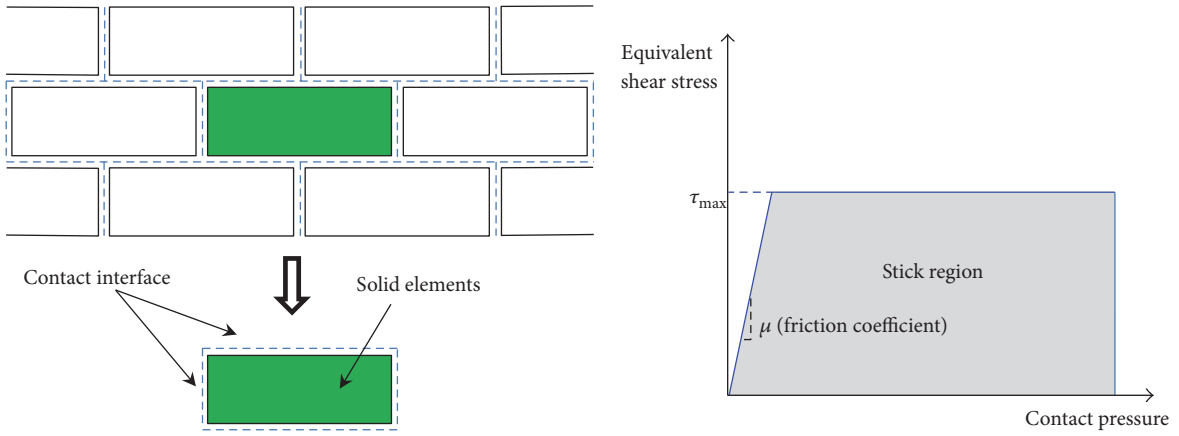

(a) Contact interfaces between the masonry blocks

(b) Schematic plot of tangential response

Figure 5: Contact behavior and details.

against the result of two previously performed experimental studies. The verification consists of comparing the failure mode and force-displacement curve of the test specimens and the corresponding numerical model. The real earthquakes pose simultaneous seismic demands under in-plane and out-of-plane directions on infilled frames, and hence few studies so far aimed at understanding the in-plane and out-of-plane interaction of infilled frames [8, 13, 50, 51]. Nonetheless, the main target of this study is to evaluate the effects of details regarding isolation of infill walls from the frame on the out-of-plane behavior of infilled frames. As a result, the effects of such isolation scheme on the in-plane behavior of infilled models are evaluated first; and in the following, the out-of-plane responses of such frames are compared.

3.3.1. In-Plane Response. To validate the modeling approach and the assumptions used in the current study, an infill wall specimen from an experimental program by Tasnimi and Mohebkhah [16] was selected for comparison. In that study, the in-plane cyclic behavior of six large-scale, single-story, single-bay specimens having different opening scheme was investigated. The control specimen SW was modeled using the above-explained approach, and the results predicted by the numerical simulation are compared with the reported experimental data. The specimen SW was a solid infill wall with 2400 mm length and 1870 mm height and consisted of 219 × 110 × 66 mm solid clay bricks placed in running bond with 22 courses within a surrounding moment-resistant steel frame. The steel frame was fabricated using IPE140 sections, having a yield stress of 315 MPa. Mortar shear strength was reported to be equal to 0.48 MPa and the average coefficient of friction of the mortar joint between the bricks units and the steel frame was 0.74. The compressive strength of masonry prism was 7.4 MPa.

Figure 6 shows the applied loading protocol and a comparison of the force-displacement envelop from the experimental test along with the corresponding results from the numerical model. As it is shown, a very good agreement between the numerical and experimental results exists. The overall level of discrepancy between the results is quite small and acceptable, and hence the same modeling approach is used hereafter.

3.3.2. Out-of-Plane Response. For calibration of the numerical simulation of infilled frames under out-of-plane loading, the experimental results of specimen E-3 carried out by Varela-Rivera et al. [17] are taken into account. The modulus of elasticity of the masonry units was equal to 1350 MPa for the specimen E-3, while the measured compressive and tensile strength were equal to 2.45 and 0.4 MPa, respectively.

Except for the mortar shear strength which was reported to be equal to 0.36 MPa, the same contact interface properties as previous sections were considered in the model. The surrounding frame was made by 19.8 MPa concrete and

Table 2: Tangential behavior of contact interfaces between masonry bricks.

Friction		Shear interface	
Friction coefficient	Contact pressure	Parameter	Value
1.50	0.5	Maximum shear stress (MPa)	0.6
0.91	1	Elastic slip stiffness	∞
0.61	2	Fraction of characteristic surface dimension	0.005

Table 3: Selected ground motion characteristics.

Ground motion	Year	PGA (g)	PGD (mm)	Duration (s)
El-Centro	1940	0.3188	213.57	31.16
Manjil	1990	0.4431	41.13	45.98
Trinidad	1983	0.1936	8.87	21.38

also the nominal yield strength for the longitudinal and transverse reinforcement was equal to 412 and 228 MPa, respectively. Figure 7 shows the failure mode of the previously tested specimen and the corresponding numerical model. In both parts of the figure, the potential lines of the concrete slabs due to confinement provided by the frame members are obvious which are represented by out-of-plane bending cracks. Also, the force-displacement of the model and that of the corresponding specimen shown in Figure 8 are in good agreement, which proves the ability of the model in capturing the response characteristics of infilled frame under out-of-plane loading.

4. Evaluation of Structural Response of the Proposed System

The evaluation of the structural responses of infilled frames in both in-plane and out-of-plane directions is presented in this section. Infilled frames with different aspect ratios (H/L = 1.0, 0.75, and 0.6) were investigated for each geometrical case mentioned in the previous section. First, results of the in-plane loading analyses were compared to ensure that the undesirable stiffening effects of the infills are properly prevented by the proposed configurations. Subsequently, out-of-plane performance of each case was examined via IDA analysis. Finally, time history analyses were conducted to examine the out-of-plane dynamic response of infilled frames against ground motions with different frequency components.

4.1. In-Plane Behavior. Cyclic displacement control analyses are conducted to predict the hysteresis behavior of different infilled frame models. Numerical models are developed for the bare frame and the frame with a full solid infill wall to identify the effectiveness of each detail on the in-plane response of the frame. Results of the infill walls with different H/L ratios are compared in Figure 9, in which a single curve is plotted for the in-plane response of Case I and Case II due to the identical in-plane characteristics. As it can be seen from Figures 9(a)–9(c), compared to the force-displacement curve for the bare frame, the proposed infill systems have successfully increased the resistance of the frame without noticeable effect on the initial stiffness. It is observed that the stiffness of the infilled frame with full contact between the infill wall and the frame is considerably larger than the corresponding isolated infilled frames. Also, the maximum strength of the bare frame is up to 35% lower than that in the corresponding full infilled frames. Similar observations were reported by Žarnić et al. [27], Jiang et al. [29], and Tasligedik [52]. The peak strengths increased up to 16% and 29% on average for Cases I and II and Case III, respectively. Similar effects on the response of each case were observed for different aspect ratios (Figures 9(a)–9(c)).

On the contrary, response of fully infilled cases showed significant increase up to 175%, in the initial stiffness in the in-plane direction, even though the average increase in the peak strength was only 32%. Full solid infill system reached its peak strength in a smaller drift, and its strength dropped noticeably afterward. This effect was more significant in models with lower H/L ratio.

4.2. Out-of-Plane Behavior. FEMA P695 [53] prescribes the IDA methodology as a reliable solution to evaluate the seismic response of structures and structural elements. This methodology includes performing time history analyses on the structure model subjected to different ground motions and with different intensities. This can eliminate the potential uncertainties in ground motion selection and scaling [53]. The out-of-plane seismic failure assessment of infilled frames is conducted for different infill wall models using IDA procedure to identify the dynamic response of each infill case. Table 3 shows the characteristics of the selected ground motions in the current study. The ground motion records are applied in different PGA levels as the intensity indicator, and the out-of-plane displacements of the wall in different levels are tracked. The dynamic damping is considered by means of mass and stiffness proportional Rayleigh damping. A damping ratio of 5% is assigned to the materials based on the frequency of the vibration for the first two modes of the structure model.

Figures 10(a)–10(c) show the results of IDA analysis of the three infilled frame models, depicting the maximum out-of-plane displacement of the infill walls in different ground motion intensities. It is observed that the infill walls with higher aspect ratios have more stable seismic response in

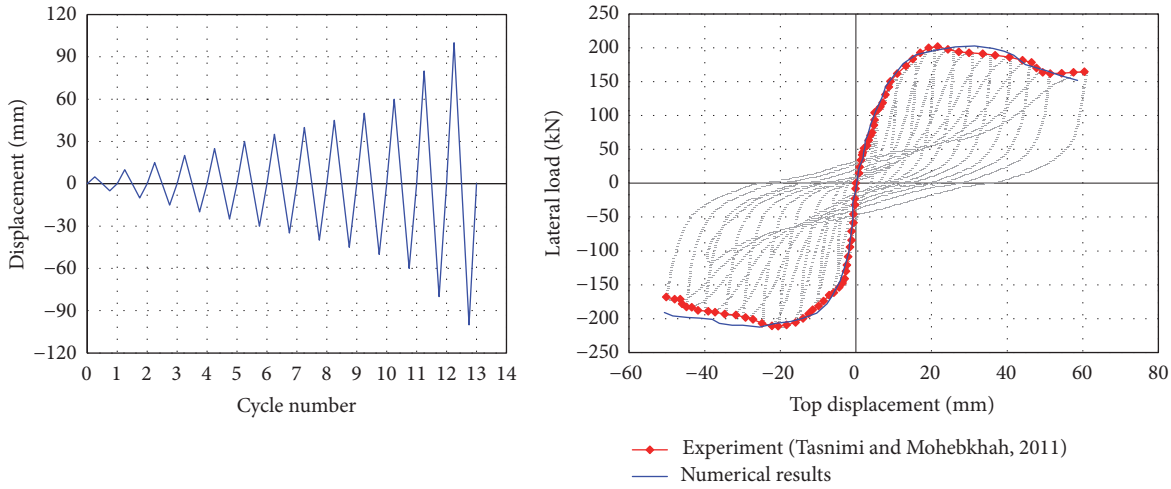

(a) Applied loading protocol

(b) Comparison of results from the numerical model and the experimental data

Figure 6: Specimen SW tested by Tasnimi and Mohebkhah [16].

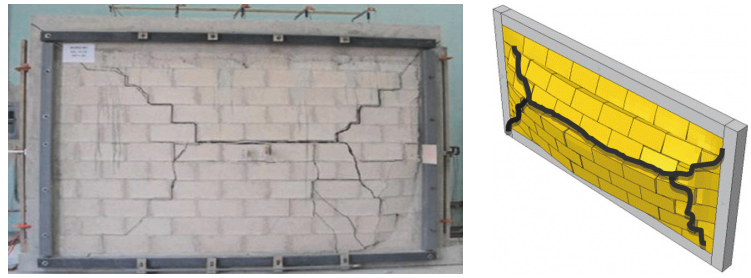

(a) Specimen's failure mode

(b) Failure mode in the numerical model

Figure 7: Damage severity and propagation in Varela-Rivera et al.'s specimen.

the out-of-plane direction. This result can be justified since all the walls have the same height and thickness but the model with $H/L = 1.0$ has shorter length than the other two. The maximum out-of-plane displacement of the infill walls for the walls with $H/L = 1.0$ is approximately 190 mm, while the corresponding values for the wall with $H/L = 0.75$ and $H/L = 0.6$ are about 90 mm and 75 mm, respectively. The latter were found to have close responses, which is because of their similar failure patterns. As for the walls with $H/L = 1.0$, shorter span means a shorter unsupported region in the infill wall, which can better prevent out-of-plane instabilities. Also, Case III is found to be the most resistant wall in all the three H/L ratios, followed by Case II and Case I as the second and third one. This can be justified by the different boundary conditions considered for the infill walls in their top edges, where Case III has a full interaction with the beam bottom flange providing a confining action on the infill wall. This creates an extra support on the top of the wall as the normal contact forces in the interface act on the wall by limiting the vertical displacements, which was recently proved to have a significant effect on the out-of-plane response of the wall [54]. The supported top edge of the wall has, therefore, an influence on the axial force to which the out-of-plane loaded wall is subjected, and hence it influences the out-of-plane response of the infill wall to have a membrane action.

As a sample of the results of the IDA analysis, displacement responses of the walls with $H/L = 0.6$ are presented in Figure 11. The maximum absolute out-of-plane displacement at three different levels along the height of the infill wall ($0.25H$, $0.5H$, and $0.75H$) is recorded for the comparison. The solid lines in this figure represent the cases which are resistant to the ground motion excitations. The dashed lines indicate the cases experiencing failure. The maximum absolute out-of-plane displacement observed in the infill wall Case I is equal to 32 mm corresponding to the PGA of 0.05 g. Case I and Case II show similar out-of-plane behaviors during the ground motion with PGA = 0.02 g. However, Case II clearly shows a more stable out-of-plane behavior by maintaining its integrity up to 46 mm out-of-plane displacement which is higher than that of Case I by 43%. The corresponding value of 87 mm for Case III indicates an increase of 171% in comparison with Case I.

Figure 12 shows a comparison of the maximum absolute out-of-plane acceleration of the wall along the height of the walls with H/L ratio of 0.6. As can be seen, in most cases, the maximum absolute out-of-plane acceleration for the infill is

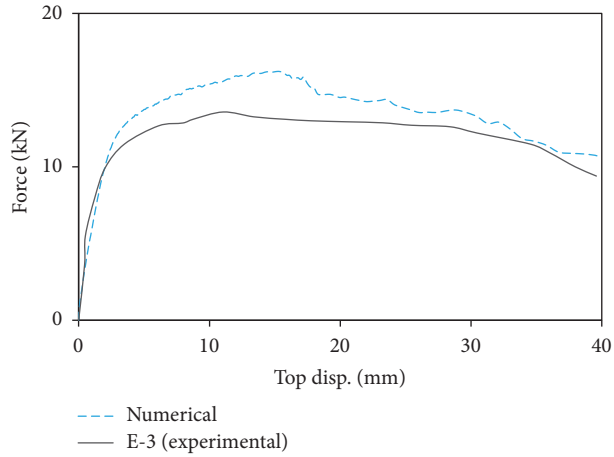

Figure 8: Comparison of force-displacement curves of the numerical and the experimental results under out-of-plane loading in Varela-Rivera et al. [17].

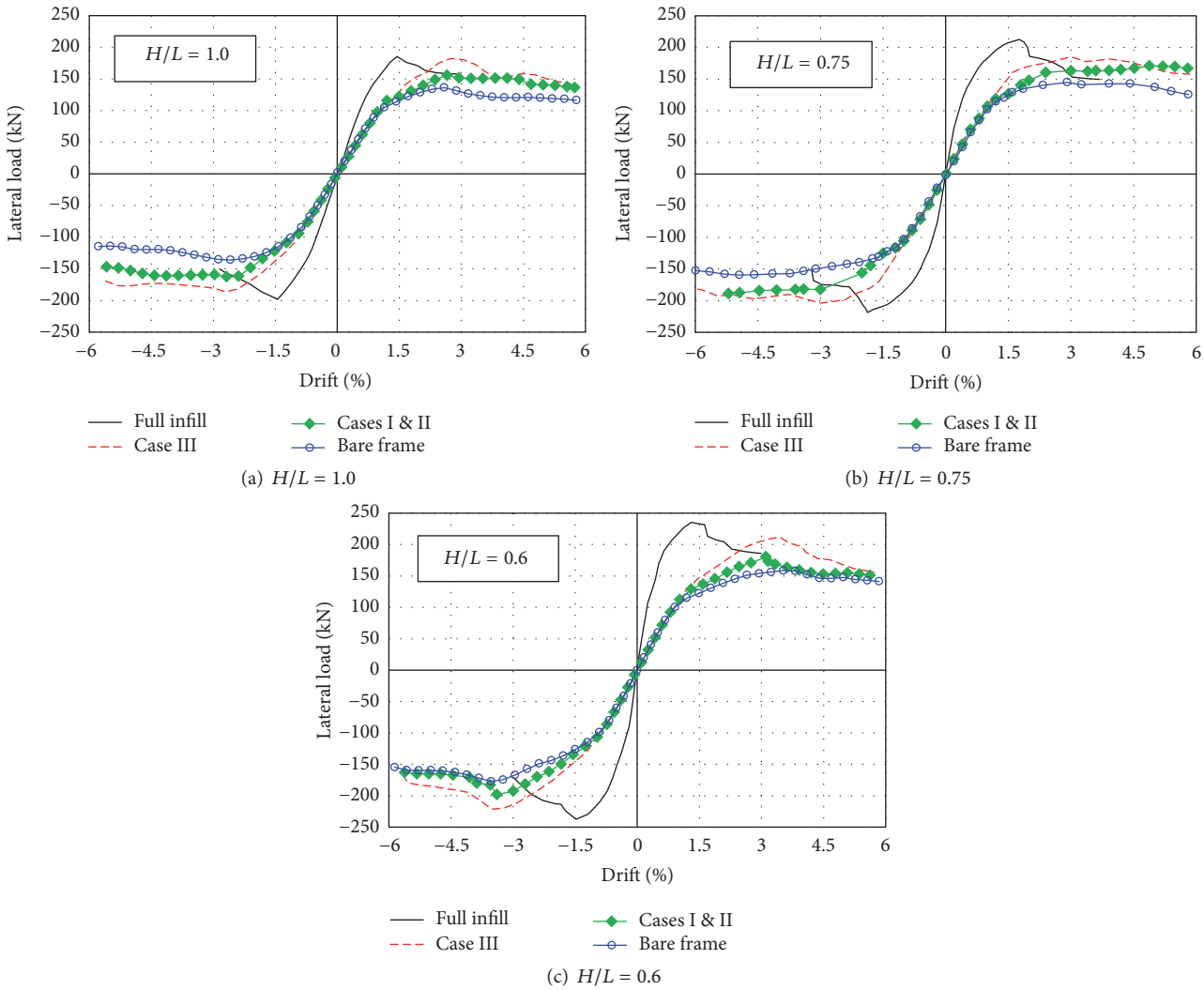

Figure 9: Cyclic response of infilled frames subjected to in-plane loading.

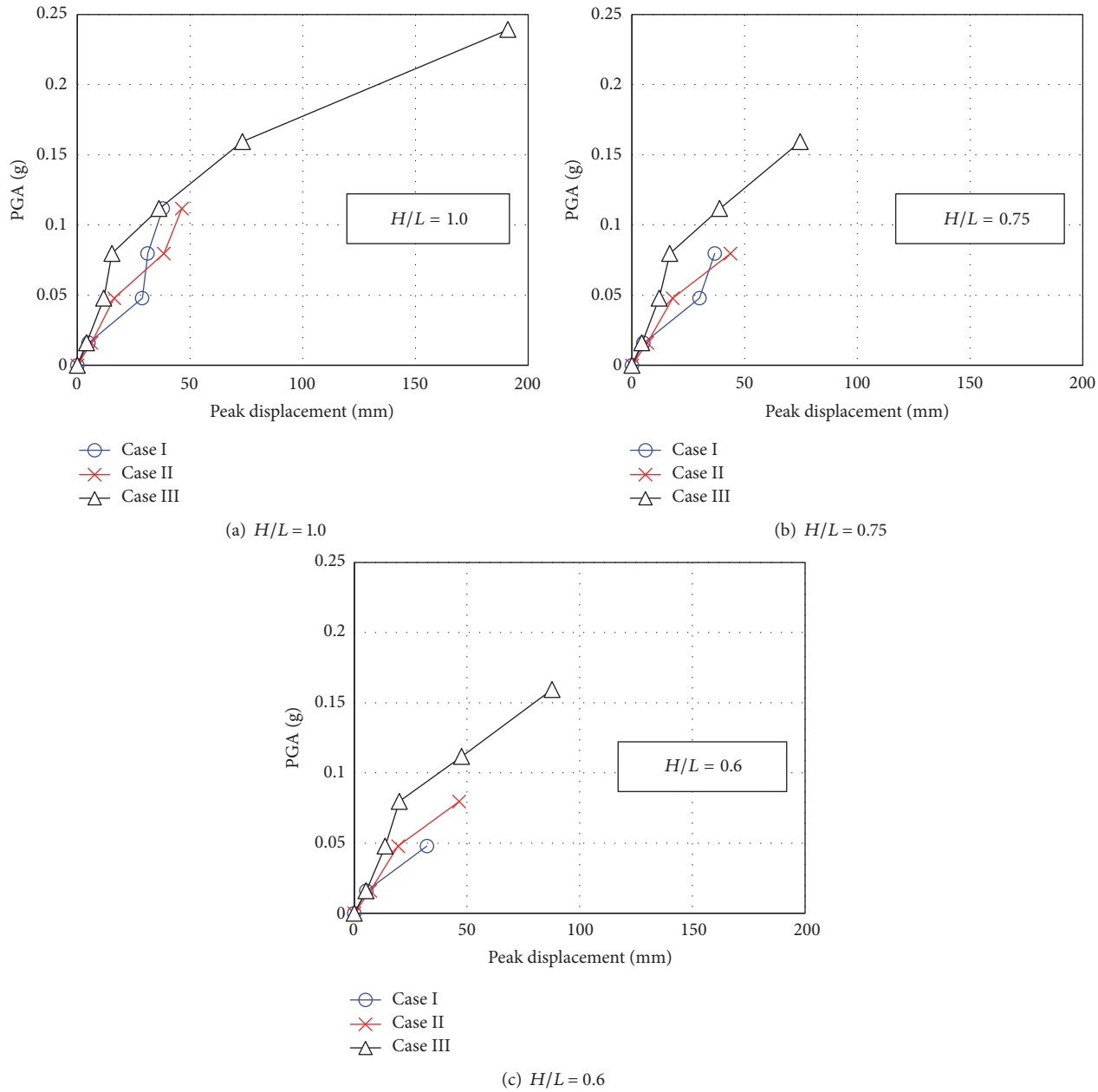

(a) $H/L = 1.0$

(b) $H/L = 0.75$

(c) $H/L = 0.6$

Figure 10: IDA results of the infill walls under El-Centro ground motion.

observed in the lower part of the infill wall, which indicates the contribution of higher modes of vibration in the time history response of each wall. Moreover, the acceleration response of each wall is found to have higher peaks than the input ground motion.

Sample deformed shapes for each configuration of the infilled walls with $H/L = 0.6$ are shown in Figure 13. It is worth mentioning that the values presented in the legend area of the contour plots in Figure 13 (the left column) correspond to the total out-of-plane displacements of the infill walls. A comparison between the failure patterns of the walls is conducted and the results are depicted in Figure 13 (the right column in which the red lines denote the major cracking between the bricks). The results of this figure show that providing the infill with more contacts and larger connection length leads to transformation of the cracked zone from the top of the infill wall to the central part. This is mainly due to fact that, in Case III, the wall is attached to the frame at the top and more steel angles attached the infill wall to the surrounding frame. As a result, arching action can be activated which greatly improves the response characteristics of the infill. As can be seen in Figures 11 and 12, this arching action has led to considerable reduction of both displacement and acceleration of the infill walls compared to other cases.

As it can be seen, for infill walls isolated from the frame on both the horizontal and vertical edges of the infill wall (Cases I and II), a failure mode other than that associated with the classical arching action is observed. As for the infill

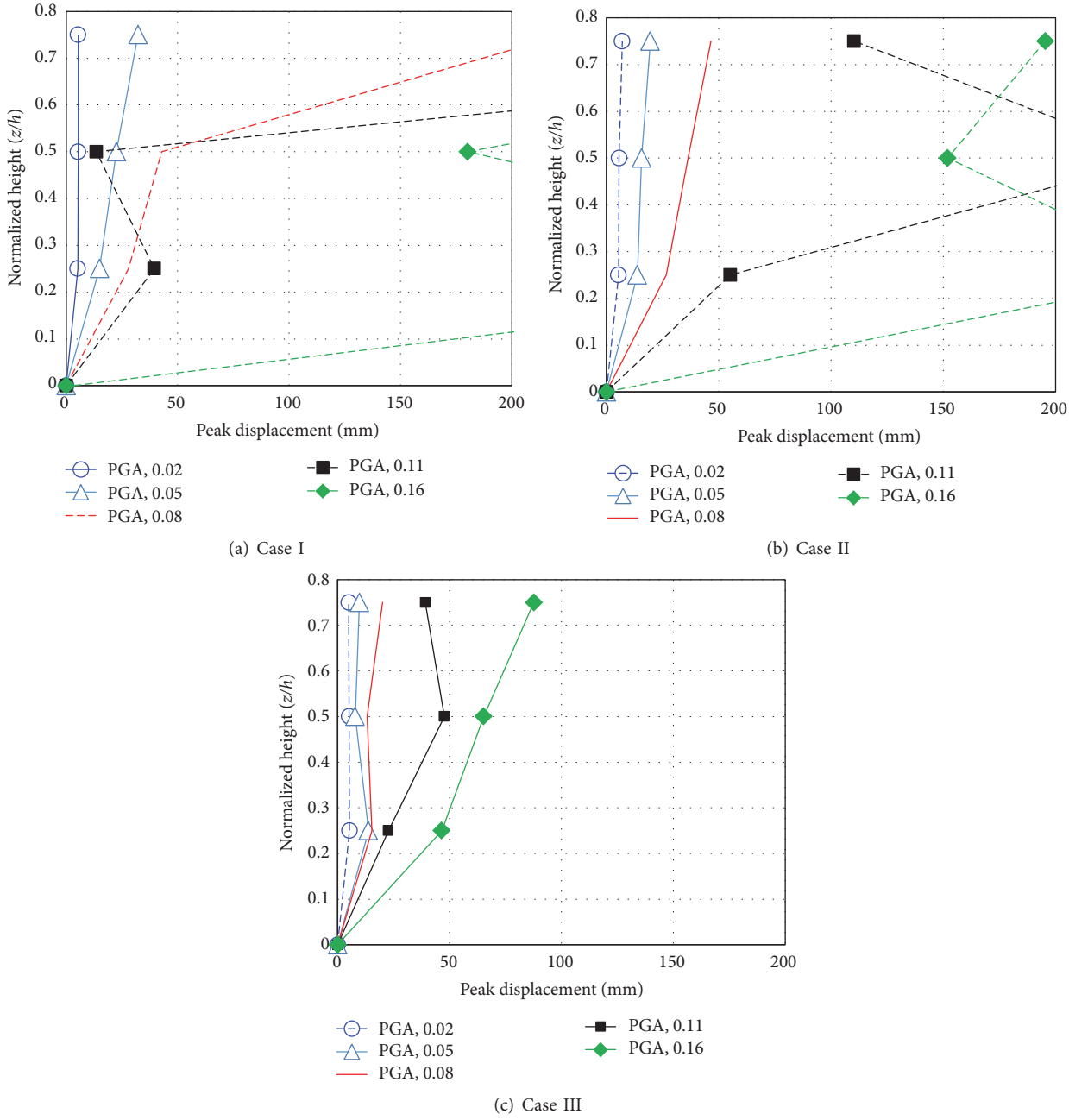

Figure 11: Displacement response of the walls under El-Centro ground motion with different intensities ($H/L = 0.6$).

walls with vertical isolation only (Case III), the observed failure pattern is found to match the expected arching action reported by other researchers [12–14]. Similar results are observed for the walls with aspect ratios of 0.75 and 1.0.

4.3. IDA Results. The results of the IDA of the infill walls with different aspect ratios are summarized in Table 4. For each intensity level of the ground motion records, the characteristics of the excitation including the Peak Ground Acceleration (PGA) and the Peak Ground Displacement (PGD) are reported as well as the infill walls responses. From the results of the IDA, infill wall Case III is found to have a more stable out-of-plane behavior and better resistance against the ground motions with higher intensity levels.

Two new sets of IDA analyses were conducted on the infill wall Case III to perform a more detailed evaluation on the out-of-plane response of this case. Considering the El-Centro record as a far field low-frequency record, relevant real earthquake scenarios of both low-frequency and high-frequency excitations are selected to conduct the investigation on the infill wall response over a range of excitations (see Table 3). For instance, the 1983 Trinidad earthquake had a relatively high PGA (0.19 g) but a small PGD (8.87 mm) indicating that this earthquake has a dominant

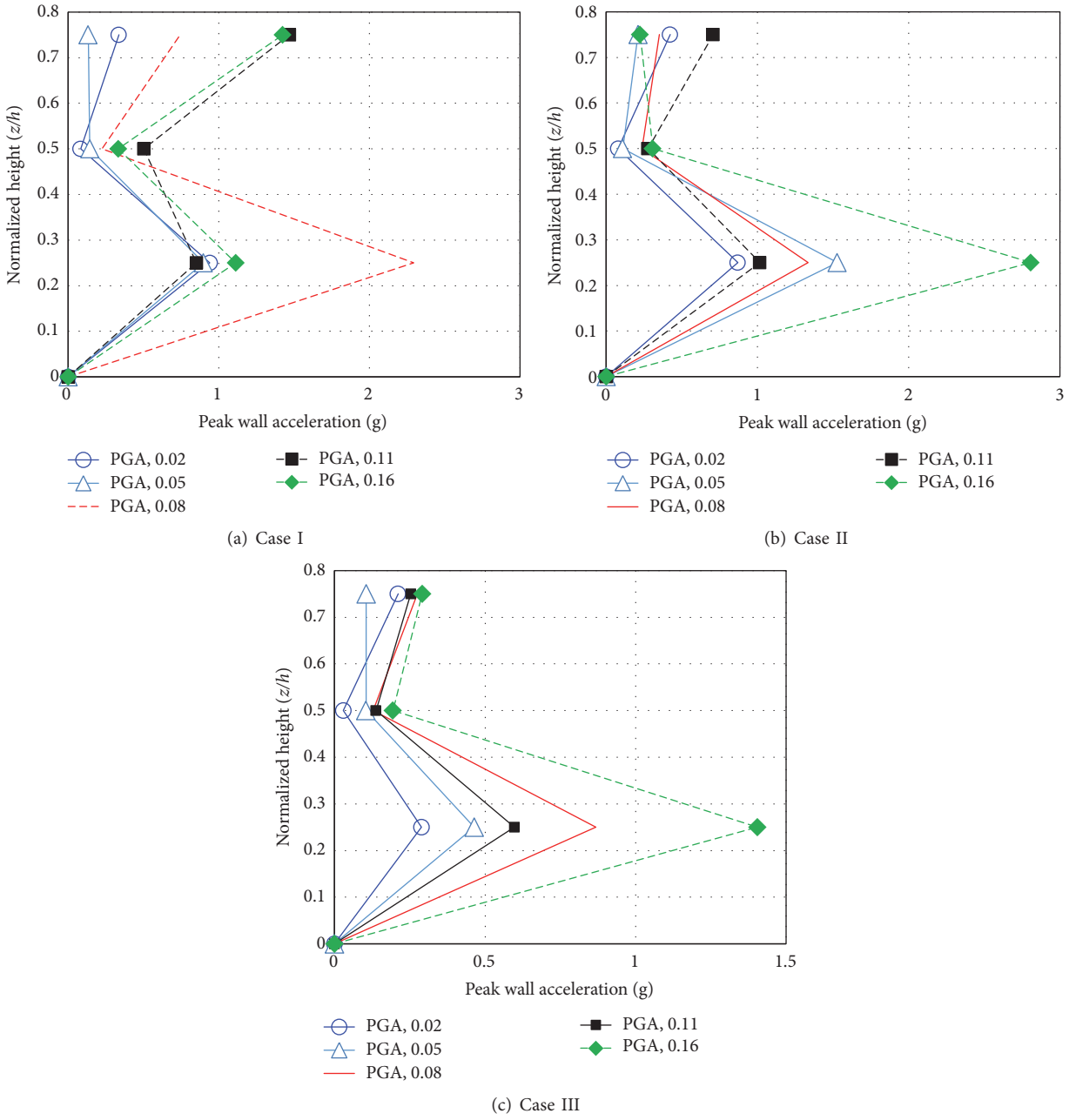

Figure 12: Acceleration response of the walls under El-Centro ground motion with different intensities ($H/L = 0.6$).

high-frequency component. This can induce severe effects on the low-rise brittle nonductile structures because of the large acceleration. Regarding the 1940 El-Centro record, high PGD and similarly large PGA indicate lower dominant frequencies. The 1990 Manjil record was also selected as an accelerogram with mid-range frequency content.

Similar IDA are conducted using the Trinidad and Manjil earthquakes. The scaled records are applied until the instability of the infill wall specimen occurred. Table 5 shows the seismic response comparison for the considered infill walls subjected to earthquake excitations with various frequency contents. The peak acceleration and displacement of the infill wall (PWA and PWD) are calculated as the maximum values measured at the $0.25H$, $0.5H$, and $0.75H$ for each test specimen.

The peak wall displacement response (PWD) and input displacements (PGD) are compared for Case III. As it can be seen from Table 5, the El-Centro earthquake with the scale factor of 0.75, giving the PGA of 0.239, results in the collapse of the infill wall because of its PGD of 160.2 mm. On the contrary, the Trinidad earthquake with the scale factor of 4.00, giving the high PGA of 0.774 g, is unable to cause failure due to its intermediate PGD ($35.5 = 4 \times 8.9$ mm), even though its PGA is much larger than that of the El-Centro record with the scale factor of 0.75. This is due to the lower PGD of the Trinidad earthquake with the scale factor of 4.00

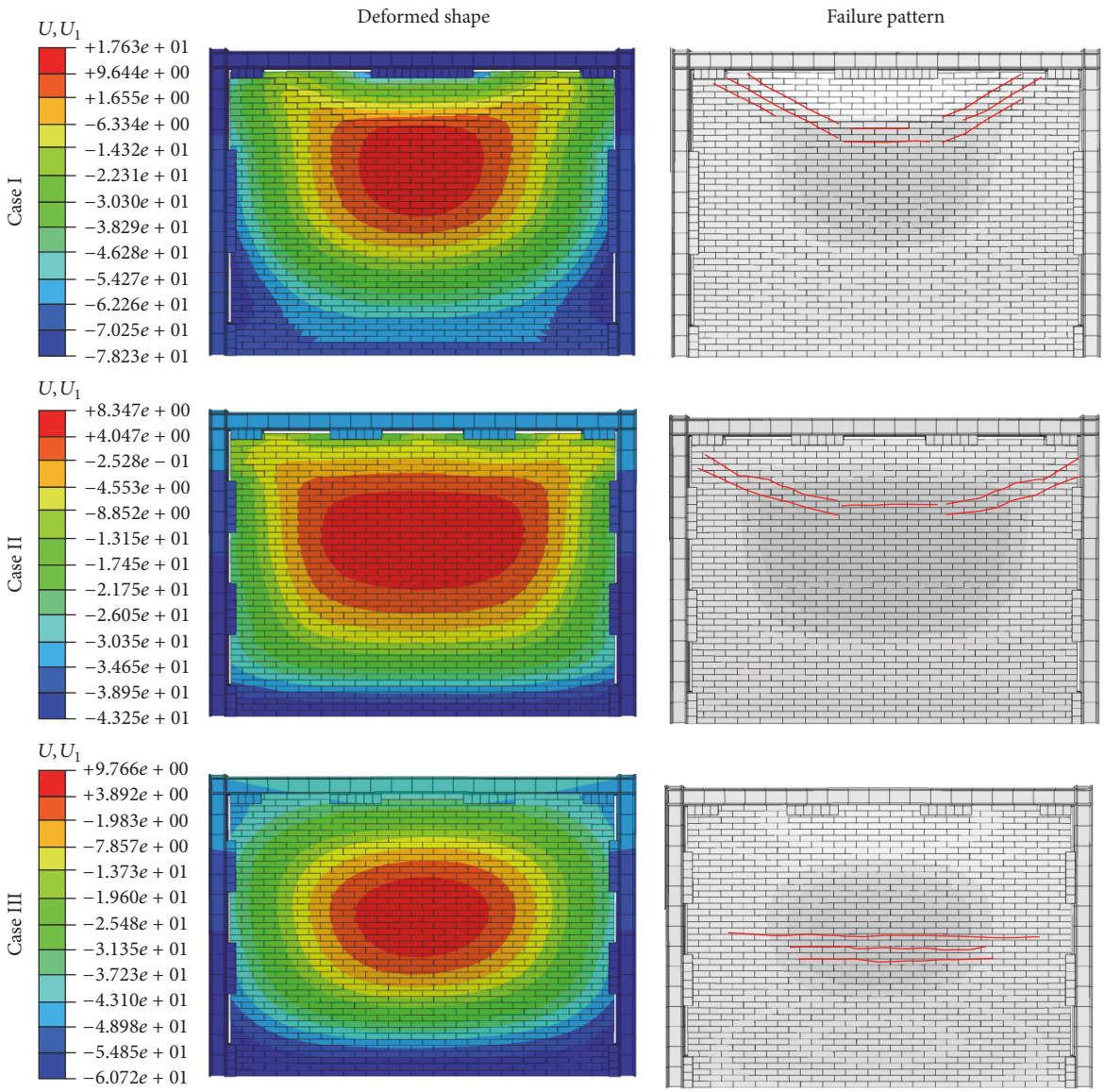

Figure 13: Deformed shape and the failure pattern of the infilled walls ($H/L = 0.6$).

in comparison with the PGD of the El-Centro with scale factor of 0.75. Similar conclusions can be made by comparing the results from the Manjil earthquake analyses. Comparison of the results for the three selected ground motion records shows that both the PGA and the PGD considerably affect the seismic response of the infill walls subjected to out-of-plane excitations. Some sample time history results of the IDA of the infill walls with $H/L = 0.6$ are presented in Figure 14. Similar results are observed for the infill walls with H/L ratios of 0.75 and 1.0.

Though the results of the current work are limited to brick masonry infill walls, many other researchers have dealt with other masonry units having different sizes and strengths. According to their results, both the stiffness and peak load of infilled frames increase with the increase of stiffness and strength of the infill [55–57]. Furthermore, in order to have stiffer infilled frame, it is preferable to use solid units rather than hollow ones [56]. These conclusions can be true for all nonisolated infill walls including those participating in the later stages of loading.

5. Conclusions

For the out-of-plane response of the infill walls, it is important to notice that the support condition of the panel can substantially affect the behavior of the masonry infills. Proper support conditions can hold the masonry wall and prevent the wall failure during out-of-plane excitations. On the other hands, support conditions should be provided such that no major variation in the in-plane behavior of the infilled frame occurs. In this study, steel frames infilled with solid masonry blocks with different aspect ratios were examined

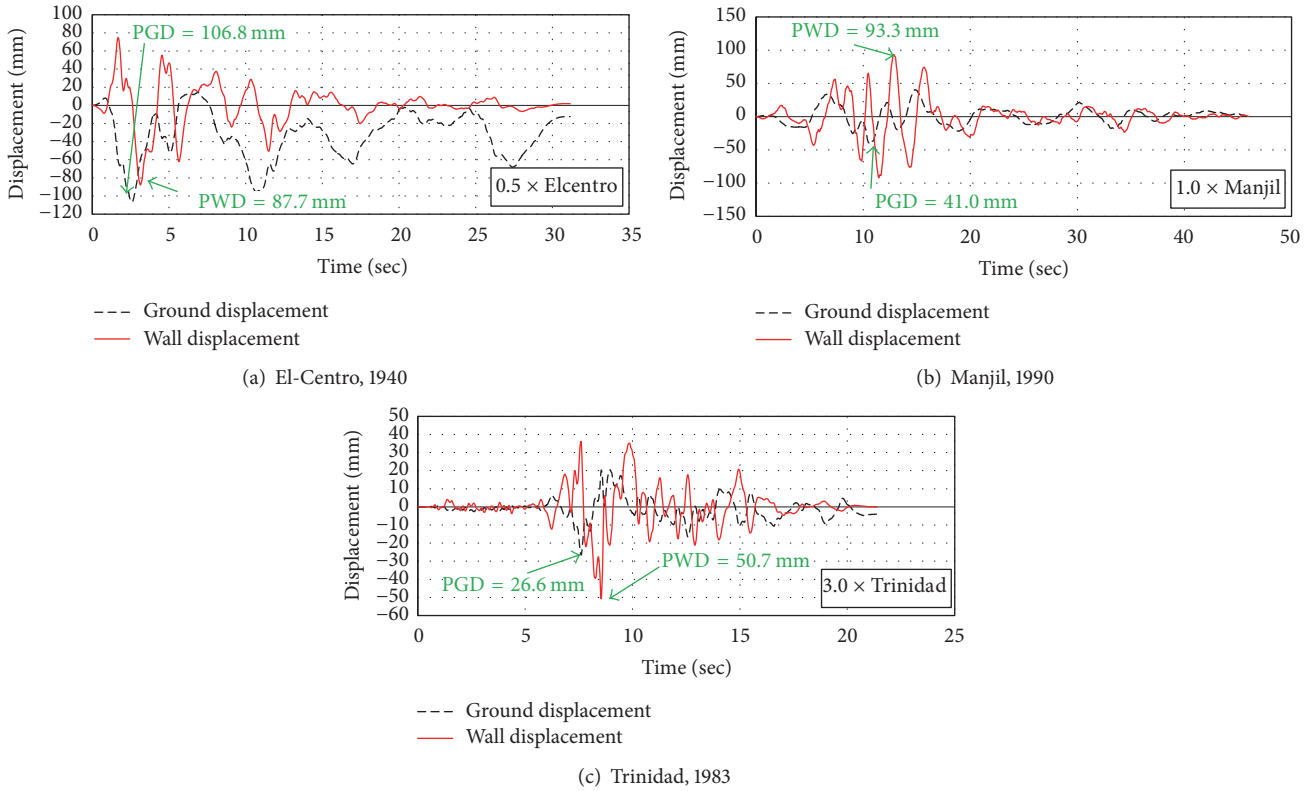

Figure 14: Sample seismic response of the considered infill walls subjected to different ground motions.

Table 4: Summary of the key IDA results for different infill configurations.

Specimen	Excitation		PGD (mm)	PGA (g)	$H/L = 1.0$		$H/L = 0.75$		$H/L = 0.6$	
					PWD[1] (mm)	PWA[2] (g)	PWD (mm)	PWA (g)	PWD (mm)	PWA (g)
Case I	5%	El-Centro	10.7	0.016	4.9	0.892	5.1	0.906	5.3	0.941
	15%	El-Centro	32.0	0.048	28.8	0.918	30.0	0.851	32.3	0.898
	25%	El-Centro	53.4	0.080	31.2	1.072	36.7	0.921	Failure	NA
	35%	El-Centro	74.7	0.112	37.9	1.465	Failure	NA	Failure	NA
	50%	El-Centro	106.8	0.159	Failure	NA	Failure	NA	Failure	NA
	75%	El-Centro	160.2	0.239	Failure	NA	Failure	NA	Failure	NA
Case II	5%	El-Centro	10.7	0.016	6.2	0.915	6.7	0.898	7.0	0.870
	15%	El-Centro	32.0	0.048	16.3	1.625	18.1	1.563	19.4	1.528
	25%	El-Centro	53.4	0.080	38.4	1.354	43.7	1.344	46.5	1.336
	35%	El-Centro	74.7	0.112	46.3	1.347	Failure	NA	Failure	NA
	50%	El-Centro	106.8	0.159	Failure	NA	Failure	NA	Failure	NA
	75%	El-Centro	160.2	0.239	Failure	NA	Failure	NA	Failure	NA
Case III	5%	El-Centro	10.7	0.016	4.1	0.379	4.4	0.366	5.3	0.289
	15%	El-Centro	32.0	0.048	11.7	0.581	12.1	0.497	13.7	0.464
	25%	El-Centro	53.4	0.080	15.3	0.972	16.8	0.723	20.0	0.868
	35%	El-Centro	74.7	0.112	36.2	1.018	39.0	0.698	47.6	0.598
	50%	El-Centro	106.8	0.159	73.2	1.503	74.7	1.467	87.7	1.405
	75%	El-Centro	160.2	0.239	191.1	1.531	Failure	NA	Failure	NA

[1]Peak wall displacement; [2]peak wall acceleration.

Table 5: Seismic response comparison for the considered infill walls subjected to earthquake excitations with various frequency contents.

Specimen	Excitation		PGD (mm)	PGA (g)	$H/L = 1.0$		$H/L = 0.75$		$H/L = 0.6$	
					PWD (mm)	PWA (g)	PWD (mm)	PWA (g)	PWD (mm)	PWA (g)
Case III	50%	Manjil	20.5	0.222	35.4	0.418	39.0	0.377	40.2	0.361
	75%	Manjil	30.8	0.332	51.7	0.425	56.1	0.371	59.7	0.369
	100%	Manjil	41.0	0.443	77.1	0.523	85.0	0.455	93.3	0.441
	150%	Manjil	61.5	0.665	80.1	0.463	Failure	NA	Failure	NA
Case III	100%	Trinidad	8.9	0.194	13.5	0.256	14.1	0.241	14.1	0.241
	200%	Trinidad	17.7	0.387	30.7	0.297	31.7	0.310	33.5	0.286
	300%	Trinidad	26.6	0.581	44.0	0.369	47.9	0.329	50.7	0.313
	400%	Trinidad	35.5	0.774	52.8	0.334	57.3	0.327	58.3	0.315

using a nonlinear finite element approach to investigate the performance of three infill support configurations. The results showed the following:

(i) Isolation of the infill wall from the surrounding frame can efficiently control the undesirable effects on the in-plane stiffness of the infilled frames.

(ii) In comparison with the bare frame, infilled frames with full infill-frame connection have a notably higher stiffness.

(iii) Different failure patterns can occur for the infill walls depending on the support conditions and the interface with the frame, which does not necessarily match the arching action reported in the literature.

(iv) Partially isolated infill walls that are isolated solely on the vertical edges were found to be the most efficient configuration for the infill walls evaluated in the current study, by which the highest out-of-plane resistance was achieved. As for the in-plane stiffness of the frame, however, no notable increase was observed in this configuration compared to the corresponding bare frame.

(v) Proper distribution of the wall's out-of-plane supports on the outer edges was found to be considerably effective in the frames with lower height-to-length ratio (e.g., $H/L = 0.6$). In the frames with higher aspect ratio ($H/L = 1.0$), this effect was negligible.

(vi) Comparison of the results for real earthquakes of both low-frequency and high-frequency contents confirmed the usefulness of PGD as a simple but robust indicator of damage in the seismic analysis of the infill walls subjected to out-of-plane excitations.

Conflicts of Interest

The authors declare that they have no conflicts of interest.

References

[1] A. B. Mehrabi, P. B. Shing, M. P. Schuller, and J. L. Noland, "Experimental evaluation of masonry-infilled RC frames," *ASCE Journal of Structural Engineering*, vol. 122, no. 3, pp. 228–237, 1996.

[2] A. Madan, A. M. Reinhorn, J. B. Mander, and R. E. Valles, "Modeling of masonry infill panels for structural analysis," *Journal of Structural Engineering*, vol. 123, no. 10, pp. 1295–1302, 1997.

[3] G. Magenes and G. M. Calvi, "In-plane seismic response of brick masonry walls," *Earthquake Engineering and Structural Dynamics*, vol. 26, no. 11, pp. 1091–1112, 1997.

[4] F. J. Crisafulli, *Seismic behavior of reinforced concrete structures with masonry infills [Ph.D. thesis]*, University of Canterbury, Christchurch, New Zealand, 1997.

[5] M. Saatcioglu, D. Mitchell, R. Tinawi et al., "The August 17, 1999, Kocaeli (Turkey) earthquake—damage to structures," *Canadian Journal of Civil Engineering*, vol. 28, no. 4, pp. 715–737, 2001.

[6] P. Ricci, F. De Luca, and G. M. Verderame, "6th April 2009 L'Aquila earthquake, Italy: reinforced concrete building performance," *Bulletin of Earthquake Engineering*, vol. 9, no. 1, pp. 285–305, 2011.

[7] H. Varum, A. Furtado, H. Rodrigues, J. Dias-Oliveira, N. Vila-Pouca, and A. Arêde, "Seismic performance of the infill masonry walls and ambient vibration tests after the Ghorka 2015, Nepal earthquake," *Bulletin of Earthquake Engineering*, vol. 15, no. 3, pp. 1185–1212, 2017.

[8] P. Morandi, S. Hak, and G. Magenes, "Simplified out-of-plane resistance verification for slender clay masonry infills in RC frames," in *Proceedings of the ANIDIS 2013-XV Convegno di Ingegneria Sismica*, 2013.

[9] M. C. Griffith and J. Vaculik, "Out-of-plane flexural strength of unreinforced clay brick masonry walls," *TMS Journal*, vol. 25, pp. 53–68, 2007.

[10] M. J. N. Priestley, "Seismic behaviour of unreinforced masonry walls," *Bulletin of the New Zealand National Society for Earthquake Engineering*, vol. 18, pp. 191–205, 1985.

[11] K. Doherty, M. C. Griffith, N. Lam, and J. Wilson, "Displacement-based seismic analysis for out-of-plane bending of unreinforced masonry walls," *Earthquake Engineering & Structural Dynamics*, vol. 31, no. 4, pp. 833–850, 2002.

[12] J. L. Dawe and C. K. Seah, "Out-of-plane resistance of concrete masonry infilled panels," *Canadian Journal of Civil Engineering*, vol. 16, no. 6, pp. 854–864, 1989.

[13] R. D. Flanagan and R. M. Bennett, "Bidirectional behavior of structural clay tile infilled frames," *Journal of Structural Engineering*, vol. 125, no. 3, pp. 236–244, 1999.

[14] P. Asteris, L. Cavaleri, F. Di Trapani, and A. Tsaris, "Numerical modelling of out-of-plane response of infilled frames: state of the art and future challenges for the equivalent strut macromodels," *Engineering Structures*, vol. 132, pp. 110–122, 2017.

[15] M. L. Moretti, "Seismic design of masonry and reinforced concrete infilled frames: a comprehensive overview," *American Journal of Engineering and Applied Sciences*, vol. 8, no. 4, pp. 748–766, 2015.

[16] A. Tasnimi and A. Mohebkhah, "Investigation on the behavior of brick-infilled steel frames with openings, experimental and analytical approaches," *Engineering Structures*, vol. 33, no. 3, pp. 968–980, 2011.

[17] J. Varela-Rivera, J. Moreno-Herrera, I. Lopez-Gutierrez, and L. Fernandez-Baqueiro, "Out-of-plane strength of confined masonry walls," *Journal of Structural Engineering*, vol. 138, no. 11, pp. 1331–1341, 2012.

[18] CEN, *EuroCode 8: Design of structures for earthquake resistance. Part 1: General rules, seismic actions EuroCode 8: Design of structures for earthquake resistance. Part 1: General rules, seismic actions and rules for buildings*, European Committee for Standardization (CEN), Brussels, Belgium, 2004.

[19] M. F. P. Pereira, M. F. Pereira, J. E. Ferreira, and P. B. Lourenço, "Behavior of masonry infill panels in RC frames subjected to in plane and out of plane loads," in *Proceedings of the 7th International Conference on Analytical Models and New Concepts in Concrete and Masonry Structures*, 2011.

[20] A. F. Mohammad, M. Faggella, R. Gigliotti, and E. Spacone, "Incremental dynamic analysis of frame-infill Interaction for a non-ductile structure with nonlinear shear model," in *Proceedings of the 2013 World Congress on Advances in Structural Engineering and Mechanics (ASEM '13)*, 2013.

[21] China Architecture and Building Press, *Code for Seismic Design of Buildings (GB50011-2010)*, Ministry of Construction of the People's Republic of China, Beijing, China, 2010.

[22] K. Hibbitt, *ABAQUS: User's Manual*, Hibbitt, Karlsson, and Sorensen. Inc., Pawtucket, RI, USA, 2013.

[23] P. Negro and A. Colombo, "Irregularities induced by nonstructural masonry panels in framed buildings," *Engineering Structures*, vol. 19, no. 7, pp. 576–585, 1997.

[24] P. Negro and G. Verzelletti, "Effect of infills on the global behaviour of R/C frames: energy considerations from pseudo-dynamic tests," *Earthquake Engineering and Structural Dynamics*, vol. 25, no. 8, pp. 753–773, 1996.

[25] K. M. Mosalam, R. N. White, and P. Gergely, "Static response of infilled frames using quasi-static experimentation," *Journal of Structural Engineering*, vol. 123, no. 11, pp. 1462–4169, 1997.

[26] K. M. Mosalam, R. N. White, and G. Ayala, "Response of infilled frames using pseudo-dynamic experimentation," *Earthquake Engineering & Structural Dynamics*, vol. 27, no. 6, pp. 589–608.

[27] R. Žarnić, S. Gostič, A. J. Crewe, and C. A. Taylor, "Shaking table tests of 1 : 4 reduced-scale models of masonry infilled reinforced concrete frame buildings," *Earthquake Engineering & Structural Dynamics*, vol. 30, no. 6, pp. 819–834, 2001.

[28] D. Markulak, I. Radić, and V. Sigmund, "Cyclic testing of single bay steel frames with various types of masonry infill," *Engineering Structures*, vol. 51, pp. 267–277, 2013.

[29] H. Jiang, X. Liu, and J. Mao, "Full-scale experimental study on masonry infilled RC moment-resisting frames under cyclic loads," *Engineering Structures*, vol. 91, pp. 70–84, 2015.

[30] P. B. Lourenco, *Computational Strategies for Masonry Structures*, Delf University Press, Amsterdam, The Netherlands, 1996.

[31] M. Dolšek and P. Fajfar, "Mathematical modelling of an infilled RC frame structure based on the results of pseudo-dynamic tests," *Earthquake Engineering & Structural Dynamics*, vol. 31, no. 6, pp. 1215–1230, 2002.

[32] A. Stavridis and P. B. Shing, "Finite-element modeling of nonlinear behavior of masonry-infilled RC frames," *Journal of Structural Engineering*, vol. 136, no. 3, pp. 285–296, 2010.

[33] I. Koutromanos, A. Stavridis, P. B. Shing, and K. Willam, "Numerical modeling of masonry-infilled RC frames subjected to seismic loads," *Computers & Structures*, vol. 89, no. 11-12, pp. 1026–1037, 2011.

[34] D. Celarec, P. Ricci, and M. Dolšek, "The sensitivity of seismic response parameters to the uncertain modelling variables of masonry-infilled reinforced concrete frames," *Engineering Structures*, vol. 35, pp. 165–177, 2012.

[35] P. G. Asteris, D. M. Cotsovos, C. Z. Chrysostomou, A. Mohebkhah, and G. K. Al-Chaar, "Mathematical micromodeling of infilled frames: state of the art," *Engineering Structures*, vol. 56, pp. 1905–1921, 2013.

[36] M. A. Hariri-Ardebili, H. Rahmani Samani, and M. Mirtaheri, "Free and forced vibration analysis of an infilled steel frame: experimental, numerical, and analytical methods," *Shock and Vibration*, vol. 2014, Article ID 439591, 14 pages, 2014.

[37] G. Campione, L. Cavaleri, G. Macaluso, G. Amato, and F. Di Trapani, "Evaluation of infilled frames: an updated in-plane-stiffness macro-model considering the effects of vertical loads," *Bulletin of Earthquake Engineering*, vol. 13, no. 8, pp. 2265–2281, 2015.

[38] P. G. Asteris, A. K. Tsaris, L. Cavaleri et al., "Prediction of the fundamental period of infilled RC frame structures using artificial neural networks," *Computational Intelligence and Neuroscience*, vol. 2016, Article ID 5104907, 12 pages, 2016.

[39] M. Aliaari and A. M. Memari, "Analysis of masonry infilled steel frames with seismic isolator subframes," *Engineering Structures*, vol. 27, no. 4, pp. 487–500, 2005.

[40] D. Abrams and D. Biggs, "Hybrid masonry seismic systems," in *Proceedings of the 15th International Brick and Block Masonry Conference*, Florianopolis, Brazil, 2012.

[41] R. S. Ju, H. J. Lee, C. C. Chen, and C. C. Tao, "Experimental study on separating reinforced concrete infill walls from steel moment frames," *Journal of Constructional Steel Research*, vol. 71, pp. 119–128, 2012.

[42] J. S. Kuang and Z. Wang, "Cyclic load tests of rc frame with column-isolated masonry infills," in *Proceedings of the 2nd European Conference on Earthquake Engineering and Seismology*, Istanbul, Turkey, 2014.

[43] C. Stallbaumer, *Design comparison of hybrid masonry types for seismic lateral force resistance for low-rise buildings [Ph.D. thesis]*, Kansas State University, Manhattan, Kansas, 2016.

[44] NZS-3101, *Code of Practice for the Design of Concrete Structures, Part 1, Standards Association of New Zealand*, Wellington, Zealand, 1995.

[45] SNIP-II-7-81, *Building Code on Construction in Seismic Areas*, The Ministry for Construction of Russia, Moscow, Russia, 1996.

[46] P. B. Lourenço, G. Milani, A. Tralli, and A. Zucchini, "Analysis of masonry structures: review of and recent trends in homogenization techniques," *Canadian Journal of Civil Engineering*, vol. 34, no. 11, pp. 1443–1457, 2007.

[47] N. M. Bekloo, "A new approach to numerical modelling of masonry structures using explicit dynamic finite element method," in *Proceedings of the 14th World Conference on Earthquake Engineering*, Beijing, China, 2008.

[48] S. Rafiei, *Behaviour of double skin profiled composite shear wall system under in-plane monotonic, cyclic and impact loadings [Ph.D. thesis]*, Ryerson University, Toronto, Canada, 2011.

[49] M. Dhanasekar and W. Haider, "Explicit finite element analysis of lightly reinforced masonry shear walls," *Computers & Structures*, vol. 86, no. 1-2, pp. 15–26, 2008.

[50] K. M. Dolatshahi, A. J. Aref, and M. Yekrangnia, "Bidirectional behavior of unreinforced masonry walls," *Earthquake Engineering & Structural Dynamics*, vol. 43, no. 15, pp. 2377–2397, 2014.

[51] N. Verlato, G. Guidi, F. da Porto, and C. Modena, "Innovative systems for masonry infill walls based on the use of deformable joints: combined in-plane/out-of-plane tests," in *Proceedings of the 16th International Brick and Block Masonry Conference*, Padova, Italy, 2016.

[52] A. S. Tasligedik, *Damage mitigation strategies for non-structural infill walls [Ph.D. thesis]*, University of Canterbury, Christchurch, New Zealand, 2014.

[53] Federal Emergency Management Agency (FEMA), *FEMA P695, Quantification of Building Seismic Performance Factors*, 2009.

[54] M. Tondelli, K. Beyer, and M. DeJong, "Influence of boundary conditions on the out-of-plane response of brick masonry walls in buildings with RC slabs," *Earthquake Engineering & Structural Dynamics*, vol. 45, no. 8, pp. 1337–1356, 2016.

[55] J. R. Benjamin and H. A. Williams, "The behaviour of one–story shear wall," *Journal of Structural Engineering Division ASCE*, vol. 84, article 1723, 1958.

[56] A. Parducci and M. Mezzi, "Repeated horizontal displacement of infilled frames having different stiffness and connection systems-experimental analysis," in *Proceedings of the 7th World Conference on Earthquake Engineering*, Istanbul, Turkey, 1980.

[57] J. Dawe, Y. Liu, and C. Seah, "A parametric study of masonry infilled steel frames," *Canadian Journal of Civil Engineering*, vol. 28, no. 1, pp. 149–157, 2001.